Structural Engineering and Mechanics, *Vol. 98, No. 1 (2026) 93-116*
https://doi.org/10.12989/sem.2026.98.1.093

Techno-Press

Comparative quasi-static analysis of the seismic performance of Piloti-type RC structures with and without seismic isolation

Mo Shi*[1], Yeol Choi[2a]

[1]School of Economics and Management, Ankang University,
92 Yucai Road, Hanbin, Ankang 725000, People's Republic of China
[2]School of Architecture, Kyungpook National University,
80 Daehak-ro, Buk-gu, Daegu 41566, Republic of Korea

(Received January 19, 2026, Revised March 17, 2026, Accepted March 18, 2026)

Abstract. As the state-of-the-art in seismic resilience evolves from basic life-safety toward damage mitigation and continuous functionality, piloti-type reinforced concrete (RC) buildings remain a critical vulnerability due to their inherent vertical irregularities. While extensive literature addresses general soft-story retrofits, few studies detail the specific plastic hinge evolution and directional isolator–column interactions required to optimize isolation strategies. To bridge this gap, this study evaluates a representative piloti-type RC prototype (Ministry of Land, Infrastructure and Transport, R.O.K.), explicitly selected because its mid-rise height, asymmetric wall layout, and column dimensions accurately represent the broader stock of vulnerable piloti structures. To ensure strict methodological reproducibility, including ASCE-41 plastic-hinge definitions, material nonlinearity parameters, and effective section properties, all modeling choices are comprehensively detailed in SAP2000. Also, distinct from dynamic earthquake simulations, this study employs displacement-controlled quasi-static analyses to systematically map capacity and collapse progression without ground motion variability. Comparative analyses in both principal directions for non-isolated and base-isolated (lead-rubber bearing) configurations reveal that the non-isolated frame develops collapse-level soft-story hinges at low displacements. On the other hand, the base-isolated model completes the prescribed displacement history without collapse by dissipating input energy through isolator hysteresis, dramatically reducing superstructure hinge demand and standardizing the inter-story drift profile. Differentiating this work from prior research, the results highlight that directional stiffness disparities and column sizing dictate energy absorption pathways as larger column sections and higher-stiffness axes significantly enhance isolator efficiency. The findings in this study provide novel, reproducible insights into typical piloti-type RC structural interactions, offering practical guidance for performance-based design in high-density urban seismic regions.

Keywords: Piloti-type RC structure; quasi-static analysis; seismic isolator; seismic performance

1. Introduction

In contemporary society, rapid urbanization has not only diminished available living spaces but also intensified the demand for multifunctional public areas that accommodate both parking and leisure activities. As cities become denser, residents face the dual challenge of limited personal

*Corresponding author, Ph.D., E-mail: shimo0204@outlook.jp
[a] Professor, E-mail: choiyeol@knu.ac.kr

Copyright © 2026 Techno-Press
http://www.techno-press.org/sem/5
ISSN: 1225-4568 (Print), 1598-6217 (Online)

(a) The concourse

(b) Villa Savoye

Figure 1. Typical Piloti-type structures

(a) Jangseong-dong -2017.11.16

(b) Jangseong-dong -2017.11.15

Figure 2. Seismic damage of Piloti-type RC buildings (2017 Pohang earthquake)

space and a lack of accessible community facilities, prompting the exploration of innovative architectural solutions. One such solution is the Piloti-type RC (reinforced concrete) structure, which elevates buildings on columns to free up ground-level space for communal use, thereby mitigating the spatial constraints imposed by high population densities [1-3]. This structural design not only provides essential parking and recreational areas but also contributes to a more sustainable urban environment by optimizing land use and improving overall urban livability.

Referring to the review of relevant sources on urban design and Piloti-type RC structures, it is clear that in high-density urban areas like those in Singapore, such designs offer a creative and efficient solution to limited ground-level space. In these environments, the elevated design of the building, where the structure is supported by columns, liberates valuable ground space that can be repurposed for parking, recreation, or other community functions. This design strategy is illustrated in the Concourse of Singapore in Fig. 1(a), which demonstrates how the Piloti-type RC structure can effectively maximize spatial usage by enabling multi-functional RC buildings under the decreasing living space in the high-density urban cities. Moreover, Fig. 1(b) shows inspiration from the iconic Villa Savoye, highlighting a conceptual approach of the Piloti-type RC structure that underscores both the architectural elegance and structural benefits of this system. By emphasizing open, accessible ground levels, the Piloti-type RC structure not only addresses the critical urban demands for additional space but also contributes to more sustainable and versatile urban environments.

Despite the innovative appeal of the Piloti-type RC structure in urban design, it faces significant concerns regarding its structural seismic performance due to the inherent vulnerabilities associated with an open ground floor. Previous studies by Wang et al. [4] and Zhang et al. [5]

(a) Structure of the seismic isolator (b) Practice of the seismic isolator

Figure 3. Seismic isolator

highlights that the absence of a robust shear wall system results in the concentration of extremely large shear forces at the base columns, making Piloti-type structures highly prone to collapse under seismic activities. Furthermore, as extensive post-earthquake empirical assessments by Nascimbene [6] indicate regarding the 2016-2017 Central Italy seismic sequence, critical structural pathologies in reinforced concrete buildings frequently trigger localized failures that can rapidly propagate into widespread damage and cascading structural collapse. This profound vulnerability to real-world seismic demands was tragically exemplified by the 2017 Pohang earthquake in the Republic of Korea [7], where many Piloti-type RC structures failed as a result of extreme base shear forces, leading to massive economic losses and significant casualties, as illustrated in Fig. 2. These widespread incidents underscore the critical demand for improved seismic resistance design measures in Piloti-type RC structures, including the integration of enhanced shear reinforcement and innovative energy dissipation systems, to ensure the safety and longevity of high-density urban infrastructures.

As an advanced seismic reinforcement strategy, the installation of seismic isolators represents a transformative approach to protecting RC structures against earthquake-induced damage by fundamentally decoupling the superstructure from ground motions. Instead of relying solely on traditional resistance methods, seismic isolation utilizes flexible bearings to absorb and dissipate earthquake energy, while the bearings extend the structural vibration period and significantly reduce transmitted base shear. Especially, Yang et al. [8] demonstrated the capacity of stiffness-softening magnetorheological elastomer (MRE) isolators to suppress vibrations in scaled buildings using active closed-loop control under simulated dynamic loads. Similarly, Kang et al. [9] investigated the multi-directional energy absorption of fiber-reinforced elastomeric isolators (FREI) compared to traditional steel-reinforced types, proving their effectiveness in standard low-rise frames. Furthermore, Warn & Ryan [10] provided a comprehensive review of passive seismic isolation, emphasizing its historical validation through full-scale shake table testing across conventional structural typologies.

However, while these foundational studies [9-11] unequivocally establish the load-reducing capabilities of various advanced isolation systems under dynamic conditions, they predominantly focus on regular building frames. Including rapid soft-story plastic hinge progression, many former studies do not explicitly address the localized failure mechanisms inherent to highly irregular Piloti-type RC structures. Addressing this specific gap, this study systematically analyzes how base isolation alters capacity boundaries and prevents collapse in a vulnerable Piloti prototype using displacement-controlled quasi-static analysis. This strategy mitigates the risk of structural

collapse by preventing the amplification of seismic forces that occur when the entire structure moves in unison. As illustrated in Fig. 3, based on the previous study of Blanford et al. [11], seismic isolators have been effectively implemented in a variety of critical infrastructures across urban centers worldwide, marking a significant shift from conventional strength-based design to a more resilient, energy-dissipating paradigm.

In this study, referring to the previous research of Shi et al. [12], a comprehensive quasi-static analysis is conducted using SAP 2000 on a typical Piloti-type RC structure, as designed by the Ministry of Land, Infrastructure, and Transport of the Republic of Korea, to evaluate both non-isolated and isolated system behaviors. The study focuses on discussing the energy consumption of seismic isolators and comparing the resulting structural lateral displacements with drifts to clearly highlight the beneficial structural effects provided by the seismic isolator. By analyzing the performance differences, this study not only aims to establish a reliable reference for future study on seismic isolators in Piloti-type RC structures but also seeks to provide valuable references for the practical applications in urban construction. The anticipated findings promise to offer crucial insights into how these systems can enhance seismic resistance while simultaneously optimizing the open space of the ground level for multi-functional uses (parking and recreational areas), thus effectively addressing the dual challenges of safety and space demand in densely populated urban environments.

2. Description of the study

2.1 Structural design

This study investigates a typical Piloti-type RC structure designed in accordance with the guidelines of the Ministry of Land, Infrastructure, and Transport of the Republic of Korea. As illustrated in Fig. 4, the building has a rectangular plan measuring 14.8 m by 13.0 m, yielding a floor area of 192.4 m². The structural framework comprises 16 columns and two types of shear walls. Specifically, 14 standard columns (C1) and general walls (W1) are distributed across the plan, while two specially designed columns (C2) and core walls (W2) are concentrated in the core area to optimize load distribution and enhance structural performance.

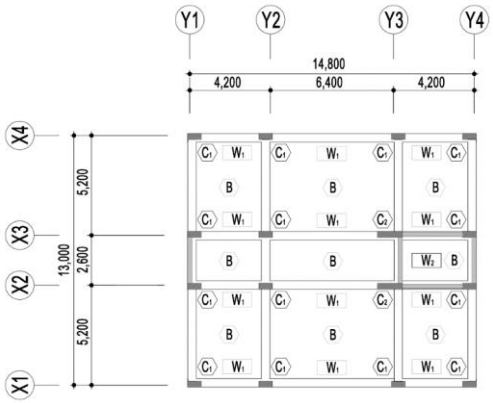

Figure 4. Floor plan

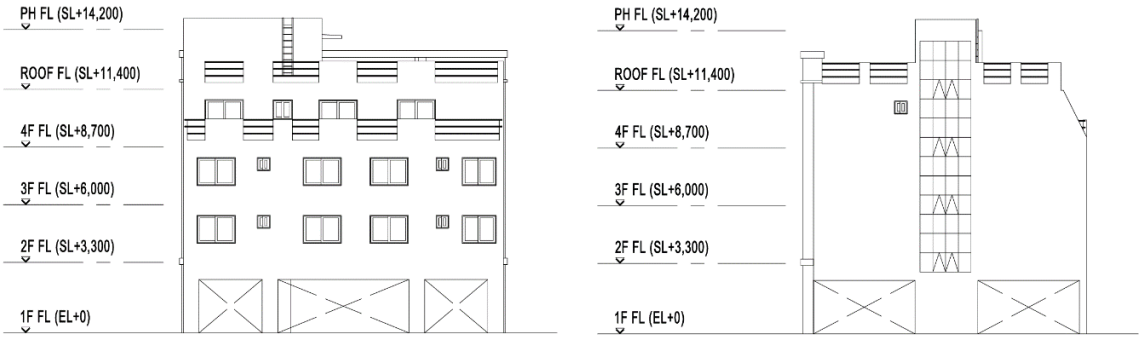

(a) Front view (b) Side view

Figure 5. Piloti-type structural elevation

Table 1. Concrete property

Weight per unit volume	25000 N/m^3
Mass per unit volume	2550 kg/m^3
Modulus of Elasticity (E)	30000 MPa
Poisson (U)	0.18
Coefficient of Thermal Expansion (A)	1.000E-05
Shear Modulus (G)	12500 MPa
Specified Compressive Strength (F_{ck})	21 MPa
Expected Compressive Strength (F_{ek})	26.25 MPa

Table 2. Rebar property

Weight per unit volume	77000 N/m^3
Mass per unit volume	7850 kg/m^3
Modulus of Elasticity (E)	200000 MPa
Poisson (U)	0.3
Coefficient of Thermal Expansion (A)	1.170E-05
Minimum Yield Stress (F_y)	400 MPa
Minimum Tensile Stress (F_u)	540 MPa
Expected Yield Stress (F_{ey})	440 MPa

Moreover, the structural elevation utilized to develop the accurate 3D SAP2000 model is shown in Fig. 5, while the structure has a total height of 14.2 m, and the first-story height is set at 3.3 m to accommodate the piloti configuration. The typical story height from the 2nd to the 5th floor is uniformly 2.7 m, and the roof stairwell has a height of 2.8 m.

2.2 Material property and section designs

The material properties of the concrete and reinforcing steel were defined in accordance with Korean standards KS F 4009:2021 and KS D 3504:2021, respectively (Tables 1, 2). For the concrete, the specified compressive strength F_{ck} is 21 MPa. To reflect realistic structural

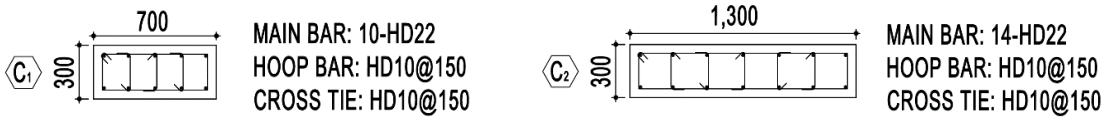

(a) Section Design C1 (b) Section Design C2

Figure 6. Column section designs

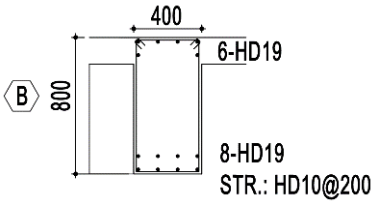

Figure 7. Beam section design

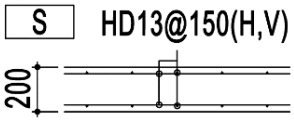

Figure 8. Slab design

performance, an expected compressive strength F_{ek} of 25.2 MPa was adopted by applying an overstrength factor of 1.2. Additionally, the concrete has a mass density of 2550 kg/m³ (unit weight of 25 kN/m³) and a Poisson's ratio of 0.18.

Similarly, the specified yield strength F_y of the rebars is 400 MPa. An expected yield strength F_{ey} of 440 MPa was utilized, based on a modification factor of 1.1. The reinforcing steel is characterized by a mass density of 7850 kg/m³ (unit weight of 77 kN/m³) and a Poisson's ratio of 0.3.

The reinforcement details and dimensions for columns, beams, slabs, and walls are illustrated in Figs. 6-9. All structural members comply with KDS 14 20 50:2022, maintaining a consistent concrete cover of 40 mm.

Regarding the components of columns and beams, two types of column sections were designed as C1 (700×300 mm^2) for general areas and C2 (1300×300 mm^2) for the core stair zone. As shown in Fig. 6, C1 is reinforced with 10-D22 longitudinal bars, while C2 employs 14-D22 bars to accommodate higher axial and bending demands. Both column types utilize D10 hoops spaced at 150 mm for confinement. According to Fig. 7, the beam section (400×800 mm^2) is unified across the structure, reinforced with 6-D19 top bars and 8-D19 bottom bars, with D10 stirrups at a 200 mm pitch.

Furthermore, the slab has a thickness of 200 mm, featuring a double-layer grid of D13 bars at 150 mm spacing in both directions, as shown in Fig. 8. For the wall systems in Fig. 9, the general wall (W1) and core wall (W2) have thicknesses of 200 mm and 250 mm, respectively. Both walls utilize a consistent reinforcement layout consisting of double-layered D13 bars arranged in a 150×150 grid to ensure structural integrity across different zones.

(a) Wall design W1 (b) Wall design W2

Figure 9. Wall designs

Table 3. Plastic hinges on column C1

Acceptance Criteria	Yield Moment kN·m	Coefficient	M2 kN·m	Yield Moment kN·m	Coefficient	M3 kN·m
IO	1688.4	0.003	1693.47	422.1	0.005	424.21
LS	1688.4	0.009	1703.60	422.1	0.045	441.09
CP	1688.4	0.010	1705.28	422.1	0.060	447.43

Table 4. Plastic hinges on column C2

Acceptance Criteria	Yield Moment kN·m	Coefficient	M2 kN·m	Yield Moment kN·m	Coefficient	M3 kN·m
IO	3135.6	0.003	3145.01	783.9	0.005	787.82
LS	3135.6	0.009	3163.82	783.9	0.045	819.18
CP	3135.6	0.010	3166.96	783.9	0.060	830.93

Table 5. Plastic hinges on beam

Acceptance Criteria	Yield Moment kN·m	Coefficient	M3 kN·m
IO	307.97	0.01	311.05
LS	307.97	0.025	315.67
CP	307.97	0.05	323.37

2.3 Plastic hinges definition

To evaluate the seismic performance of the Piloti-type RC structure, nonlinear behavior was simulated by assigning plastic hinges to structural components in SAP2000, following the ASCE 41-13 framework [13-15]. This modeling approach is essential for capturing the inelastic response and failure mechanisms observed in similar structures during the 2017 Pohang earthquake [12].

Referring to Tables 3, 4, column nonlinearity was modeled using interacting P-M2-M3 hinges to account for the coupling between fluctuating axial loads and biaxial bending moments. The modeling parameters and numerical acceptance criteria were derived from Table 10-8 of ASCE 41-13 (Condition ii: Flexure/Shear), ensuring an accurate representation of the 3D yield surface. As shown in Table 5, the beams utilize the uniaxial M3 flexural hinges, which were defined according to Table 10-7 of ASCE 41-13 to capture rotational ductility and flexural yielding.

Regarding the performance evaluation in this study, the structural response was assessed using

Table 6. Property of the seismic isolator

Direction *z*	Effective Stiffness (kN/mm)	2100
Direction *x*	Effective Stiffness (kN/mm)	0.84
	Stiffness (kN/mm)	10.94
	Yield Strength (kN)	63
	Post Yield Stiffness Ratio	0.0768
Direction *y*	Effective Stiffness (kN/mm)	0.84
	Stiffness (kN/mm)	10.94
	Yield Strength (kN)	63
	Post Yield Stiffness Ratio	0.0768

three discrete performance levels defined in ASCE 41-13: Immediate Occupancy (IO), Life Safety (LS), and Collapse Prevention (CP) [16-20]. These states served as the numerical thresholds for quantifying the damage extent and safety margins of the RC components during the nonlinear quasi-static analysis.

2.4 Definition of the boundary conditions

Based on the definition of the plastic hinges in this study, the connections between columns and beams were explicitly defined to capture the frame's inelastic response. However, the interface between the foundation and columns is equally critical, as it significantly influences the rocking component that can compromise the performance of both the superstructure and the base isolators [21-23]. Extensive research has demonstrated that the rotational behavior and energy dissipation of rocking foundations are pivotal in determining the overall seismic demand of a system [22-23]. Furthermore, the inclusion of Soil-Structure Interaction (SSI) and soil deformability has been shown to increase structural deformations and alter the dynamic characteristics of low-rise buildings [22].

Despite these potential effects, a fixed-base connection was adopted between the foundation and columns in this study for the quasi-static analysis, while this simplification was intentionally implemented to isolate the mechanical characteristics of the lead-rubber bearings (LRBs). By assuming a rigid base, this study effectively eliminates the interference of soil-induced displacements and rocking-related rotations, thereby ensuring that the evaluation of the LRBs' mechanical properties remains focused and consistent under controlled simulation requirements. This approach aligns with the need for precise performance quantification of isolation systems before considering the complex, multi-variable influence of deformable supporting environments.

2.5 Design of the seismic isolator

In this study, Lead Rubber Bearings (LRBs) were employed to enhance the seismic resilience of the Piloti-type RC structure, leveraging their proven energy dissipation and decoupling capabilities [24-28]. The LRB configuration, consisting of interleaved rubber layers and a lead core (Fig. 3(a)), effectively reduces seismic force transmission to the superstructure. The mechanical properties of the isolators are summarized in Table 6. In the vertical (*z*) direction, the isolator was modeled as linear elastic with an effective stiffness of 2100 kN/mm. In the horizontal

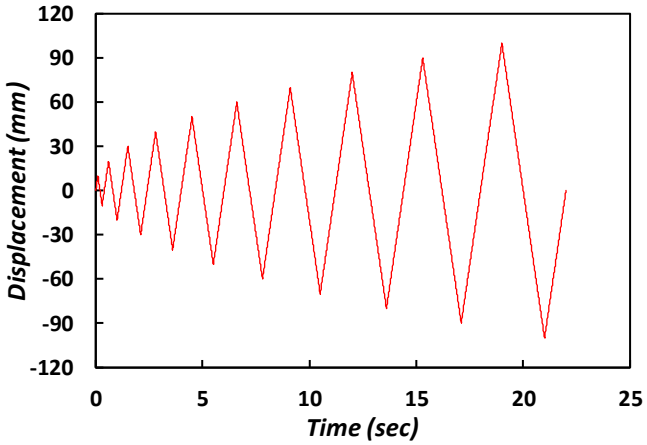

Figure 10. Time-history curve of the quasi-static analysis

(*x* and *y*) directions, a nonlinear bilinear model was implemented to characterize the hysteretic response. The initial and effective horizontal stiffnesses were defined as 10.94 kN/mm and 0.84 kN/mm, respectively. Furthermore, a yield strength of 63 kN and a post-yield stiffness ratio of 0.0768 were assigned to accurately simulate the energy dissipation during lateral excursions.

2.6 Quasi-static analysis

In accordance with the findings of Shi et al. [29], which emphasize that both dead and live loads critically dictate the initial stress state and subsequent nonlinear response in quasi-static assessments, this study adopts the load magnitudes specified in the Korean Design Standard KDS 41 10 15:2019. Specifically, as illustrated in Table 3.2-1 of KDS 41 10 15:2019, a dead load of 7.0 kN/m² and a live load of 5.0 kN/m² were applied to establish a realistic gravity pre-load. To ensure the load combination is representative of the structural mass expected during a seismic event, the gravitational combination was defined as:

$$LC = 1.0 \cdot DL + 0.25 \cdot LL \tag{1}$$

where *LC* is load combinations, *DL* indicates Dead Load, and *LL* indicates Live Load.

The specific combination in this study follows the KISTEC 2021 evaluation code for existing buildings. The 0.25 factor for live loads accounts for the sustained portion of the live load likely to be present during an earthquake, distinguishing it from peak design loads used for pure gravity analysis. Upon Eq. (1) above, accurately implementing this combination is essential for defining the P-Delta effects and the initial yielding sequence of the plastic hinges before the inception of lateral displacement-controlled loading.

As Fig. 10 illustrates, the quasi-static analysis in this study is executed through a displacement-controlled time-history curve that incrementally motivates the structural displacement from 0 mm to 100 mm over a total duration of 22 s, with each 1 mm step applied every 0.01 s. This design of the quasi-static analysis ensures that inertial effects remain minimal, thereby approximating static conditions, while still capturing nonlinear behaviors such as plastic hinge formation and energy dissipation. Furthermore, this study also underscores the necessity of conducting separate quasi-static simulations along both the *x* and *y* directions, in order to fully

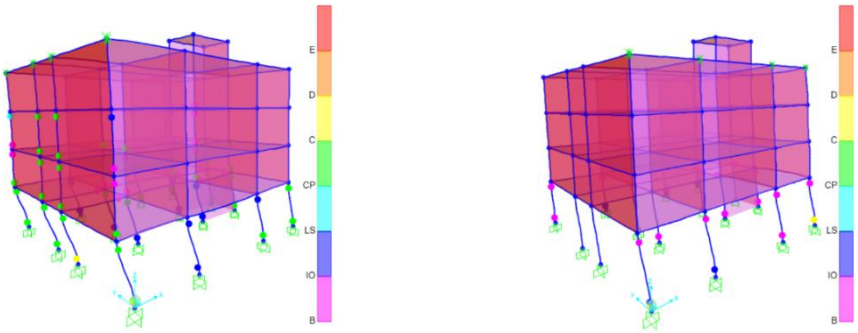

(a) Direction *x* (43 mm) (b) Direction *y* (18 mm)

Figure 11. Collapse point of the Piloti-type RC structure without the seismic isolator design

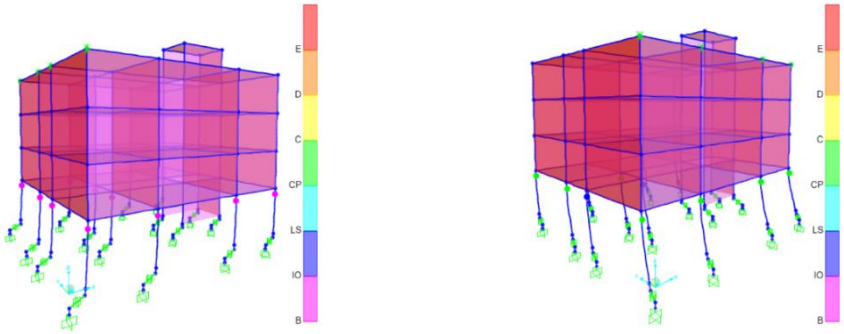

(a) Direction *x* (100 mm) (b) Direction *y* (100 mm)

Figure 12. Deformation of the Piloti-type RC structure with the seismic isolator design

capture how seismic isolators modify lateral stiffness, energy dissipation, and drift reduction in a Piloti-type RC structure, thereby analyzing the structural influence of seismic isolators under the quasi-static analysis based on the different analytical directions.

3. Discussions

3.1 Plastic hinges

The nonlinear response of the structure is governed by the plastic hinge properties defined per ASCE 41-13 (Tables 10-7 and 10-8). As indicated by Abass and Jarallah [30], the moment-rotation relationships of these hinges dictate the formation of global sway mechanisms and structural instability.

In CASE-1 (Fixed-base), plastic hinges concentrated at the ground-story columns (Fig. 11), triggering a soft-story collapse mechanism. A pronounced directional disparity was observed in this study, while collapse occurred at a displacement of 43 mm (5.43 sec) in the *x* direction but at only 18 mm (0.58 sec) in the *y* direction. This anisotropy stems from the lower lateral stiffness and shear resistance along the *y* direction, which exacerbates the soft-story effect.

Table 7. Comparison results on direction *x*

		CASE-1		CASE-2	
		Yielding	Collapse	Yielding	Collapse
Time	sec	0.05	5.43	13.6	-
Displacement	mm	5	43	80	-

Table 8. Comparison results on direction *y*

		CASE-1		CASE-2	
		Yielding	Collapse	Yielding	Collapse
Time	sec	0.05	0.58	4.42	-
Displacement	mm	5	18	42	-

In CASE-2 (Base-isolated), the isolation layer accommodated the majority of the 100 mm imposed displacement, effectively shielding the superstructure (Fig. 12). According to Ní Choine [31], this decoupling reduces base shear and flexural demands, preventing any superstructure hinges from reaching the critical Collapse (C) state. While hinges at the ground-floor columns reached the CP (Collapse Prevention) level in the *y* direction, those in the *x* direction remained at B (Yielding) or IO (Immediate Occupancy) levels. This direction-dependent performance aligns with the research, emphasizing that the architectural layout of piloti structures necessitates directional tuning of the isolation system [32-33].

Quantitative results in Tables 7, 8 further demonstrate the efficacy of the isolation design. In the *x* direction, the onset of yielding (State B) was delayed from 5 mm (0.05 sec) in CASE-1 to 80 mm (13.6 sec) in CASE-2. Similarly, in the *y* direction, yielding was deferred from 5 mm (0.05 sec) to 42 mm (4.42 sec). By dissipating energy and limiting hinge escalation, the seismic isolators significantly enhanced the displacement capacity and structural integrity of the building, preventing global collapse under major seismic demands.

3.2 Structural displacement

In displacement-controlled quasi-static analysis, tracking lateral displacement at successive stories reveals critical stiffness irregularities, such as the soft-story effect introduced by an open ground floor of the Piloti-type RC structure, which concentrates damage at particular stories. By considering the first C-state plastic hinge formation in CASE 1 to specific displacement and time points (43 mm/5.43 s in *x* direction and 18 mm/0.58 s in *y* direction), the analysis quantifies the structural lateral displacement for the Piloti-type RC structures without and with the seismic isolator designs under displacement-controlled quasi-static analysis. In this part of the discussion, Fig. 13 contrasts the displacement results of CASE-1 (without seismic isolator design) against CASE-2 (with seismic isolator design), clearly showing the structural influences due to the seismic isolator design for the specific Piloti-type RC structure.

As Fig. 13 presents, the peak lateral displacement profiles of the structure along the height in both the *x* and *y* analytical directions at the target roof displacement of 100 mm.

In the *x* direction (Fig. 13(a)), the base-isolated structure (CASE-2) exhibits a clear mechanical separation at the foundation, yielding a substantial first-story lateral displacement of 32.03 mm at the isolation layer, while the superstructure moves uniformly with minimal inter-story deformation

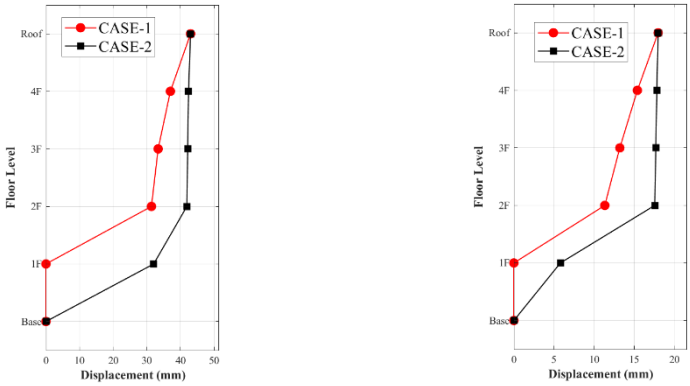

(a) Direction *x* (b) Direction *y*

Figure 13. Structural displacement

above the isolation layer. In contrast, the fixed-base, non-isolated structure (CASE-1) displays 0mm displacement at the ground level but a drastic jump to 31.36 mm at the second floor. Consistent with Fakih et al. [34], this demonstrates that the low horizontal stiffness and hysteretic energy dissipation of the isolators effectively absorb seismic input, decoupling the superstructure from ground motion and lengthening its fundamental period [35].

Similar behavior is observed in the *y* direction (Fig. 13(b)). Under the applied lateral demands, CASE-2 isolates the upper frame by accommodating a 5.81 mm displacement at the isolation interface. Consequently, it achieves a more uniform distribution of lateral displacements across the upper stories compared to the rigidly connected CASE-1, mitigating the concentration of deformation [36].

A critical vulnerability of Piloti-type RC structures is the vertical stiffness irregularity introduced by the open first story, which typically acts as a soft story, while this stiffness transition forces structural deformations to concentrate at the second-floor interface rather than the ground level. CASE-1 clearly reproduces this phenomenon, showing severe displacement gradients at the lower levels in both directions. However, the majority of the lateral movement is absorbed by the isolation layer for CASE-2, reducing the average upper-story displacements to approximately 10.33 mm and 11.98 mm in the *x* and *y* directions, respectively. Such as the 2017 Pohang event, post-earthquake reconnaissance has identified these concentrated soft-story displacements as primary drivers of localized column shear failure [37, 38]. The displacement profiles in Fig. 13 confirm that the flexibility of seismic isolators provides a robust mechanism to redistribute these demands, protect the vulnerable open-plan columns, and substantially enhance the overall seismic resilience of Piloti-type RC structures.

3.3 Story drift ratio

The story drift of the Piloti-type RC structure is a crucial parameter for evaluating the structural performance, especially in the context of comparing configurations with and without seismic isolators. Story drift quantifies the relative lateral movement between adjacent floors and serves as a key indicator of potential damage concentration, particularly in soft-story structures like the Piloti-type RC structure, which features an open ground level. Based on the discussion of the

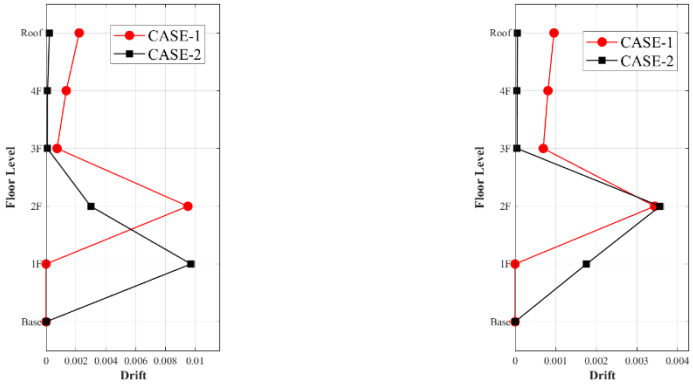

(a) Direction *x* (b) Direction *y*

Figure 14. Story drift ratio

plastic hinge for the Piloti-type RC structure without the seismic isolator design reaching the C state at a displacement of 43 mm and time 5.43 s in the *x* direction, and 18 mm at 0.58 s in the *y* direction, it is evident that these thresholds mark critical points of structural vulnerability. Using the analytical results of the structural lateral displacement, the story drift can be calculated using the Eqs. (2)-(3) below:

$$\Delta = \delta_x - \delta_{x-1} \tag{2}$$

$$\Delta_{ratio} = \frac{\Delta}{h} \tag{3}$$

where, δ_x refers to the lateral displacement recorded at the *x*-th floor, while δ_{x-1} represents the displacement at the floor immediately below it. Moreover, Δ denotes the story drift, which is simply the difference between these two displacements. The value of h in the Eq. (3) stands for the vertical height of the story being analyzed. To normalize this drift and make it a dimensionless quantity suitable for performance assessment, it is divided by the story height h, resulting in the drift ratio Δ_{ratio}. This drift ratio is especially important in performance-based seismic design because it provides a standardized measure of inter-story deformation. Regarding assessing the Piloti-type RC structure without and with the seismic isolator design in this study, the drift ratio plays a pivotal role in identifying potential weak stories and evaluating the effectiveness of seismic isolation systems.

As shown in Fig. 14, the analytical results illustrate how the seismic isolation design markedly alters the inter-story drift profiles of the Piloti-type RC structure in both analytical directions. Story drift ratio is a primary metric for assessing inelastic deformation and structural damage in performance-based seismic design, typically evaluated against established performance limit states [39, 40].

In the *x* direction (Fig. 14(a)), the non-isolated structure (CASE-1) experiences a maximum 2nd-story drift ratio of 0.0095. This value closely approaches the typical Immediate Occupancy (IO) limit state of 1.0% defined by structural technical literature in ASCE 41-13, indicating the potential onset of minor structural yielding or non-structural damage. In contrast, the base-isolated structure (CASE-2) effectively shifts the deformation demand to the isolation layer at the ground floor, which exhibits a lateral displacement of 32.03 mm and a drift ratio of 0.0097. This

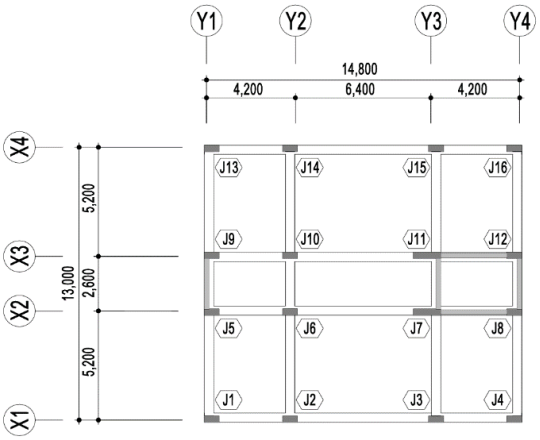

Figure 15. Placements of the seismic isolators

mechanical separation at the foundation dissipates substantial seismic energy and decouples the superstructure from ground motion, while the 2nd-story drift ratio is significantly reduced to 0.0067, keeping the upper structural elements further within the safe, elastic range.

A similar mechanical decoupling effect is observed in the *y* direction (Fig. 14(b)). While the absolute lateral displacements at the 2nd story are comparable between the two cases, their drift demands differ notably, as CASE-1 reaches a 2nd-story drift ratio of 0.0034, whereas CASE-2 mitigates this demand to 0.0018, accommodating the remaining displacement at the isolation layer (1F drift of 0.0017). Although the responses of both cases remain well below the 1.0% IO limit state in this direction, the isolation system effectively minimizes inter-story deformations. Consistent with previous studies [41, 42], limiting the drifts with LRB is crucial for reducing the demand on critical elements and enhancing the overall seismic resilience of Piloti-type RC structures.

3.4 Deformation and shear of the seismic isolator

Based on the floor plan of the specific Piloti-type RC structure, the behavior and performance of seismic isolators can be analyzed under quasi-static analysis in this study. In Piloti-type RC structures, where the ground floor is open and supported by discrete columns, isolators are positioned directly beneath each column to maximize uniform load transfer from the superstructure to the foundation, as Fig. 15 shows. This column-underlay configuration facilitates even shear load distribution across the isolation interface and minimizes plan irregularities in torsional response, which can otherwise amplify differential displacements during seismic actions. Fig. 15 illustrates the adopted floor-plan layout, where each isolator location corresponds to the centroid of its supported column footprint on the foundation, which indicates symmetric placement to reduce local stress concentrations and avoid eccentric loading. By situating isolators at these predetermined positions, the design achieves optimized performance in terms of seismic energy dissipation, serviceability, and overall structural integrity under quasi-static analysis.

As shown in Fig. 16, the quasi-static analysis in the *x* direction reveals that all seismic isolators effectively dissipate seismic energy, while the performance of the seismic isolators varies significantly with section size. Isolators paired with the smaller C1 columns (Joints 1, 2, 3, 4, 5, 6,

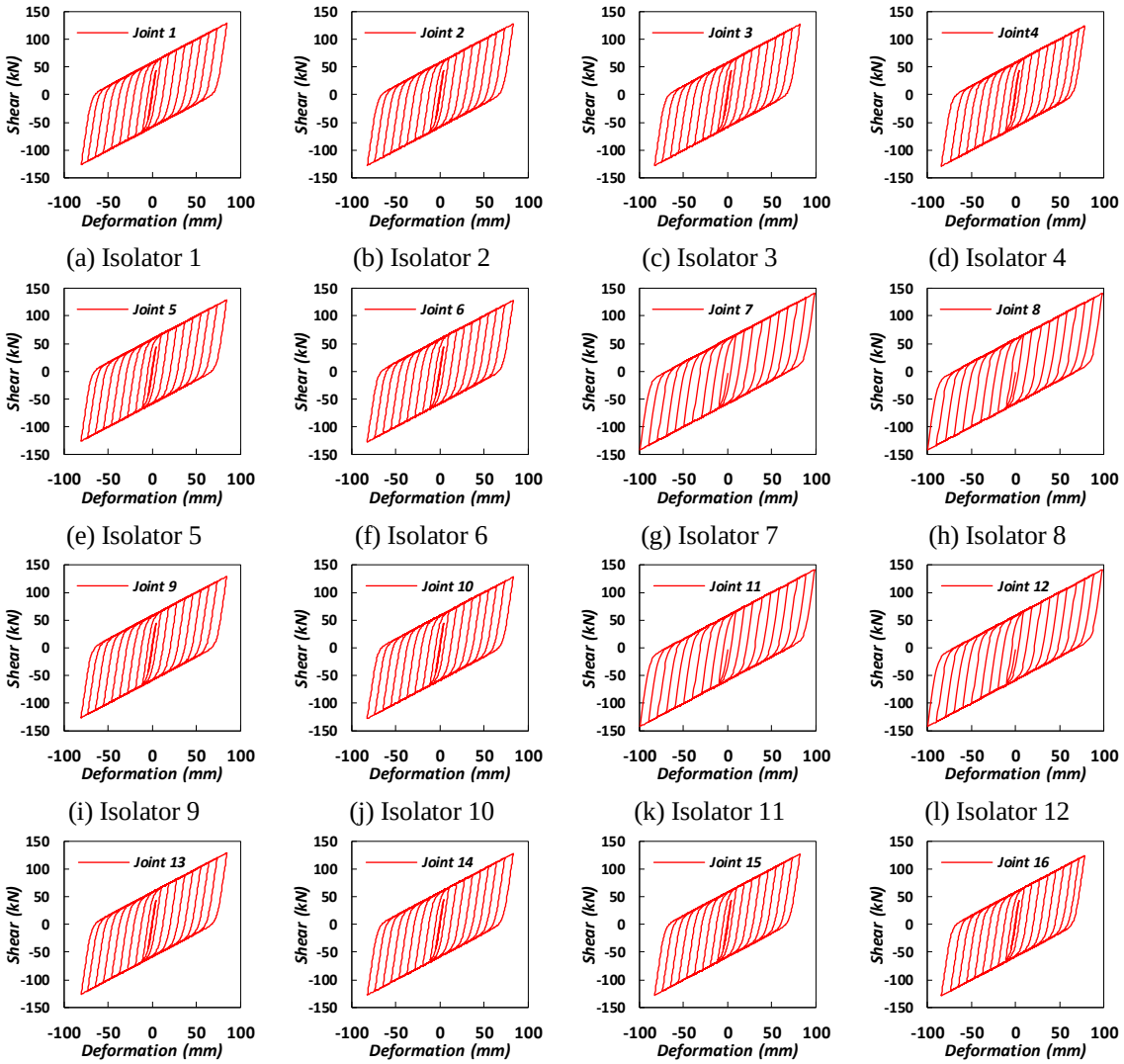

(a) Isolator 1 (b) Isolator 2 (c) Isolator 3 (d) Isolator 4

(e) Isolator 5 (f) Isolator 6 (g) Isolator 7 (h) Isolator 8

(i) Isolator 9 (j) Isolator 10 (k) Isolator 11 (l) Isolator 12

(m) Isolator 13 (n) Isolator 14 (o) Isolator 15 (p) Isolator 16

Figure 16. Behavior of seismic isolators in the *x* direction

9, 10, 13, 14, 15, 16) develop lower shear forces and exhibit less relative energy dissipation because their lower stiffness reduces sliding displacement and hysteretic loop area under the same load amplitude. By contrast, isolators under the larger C2 columns (Joints 7, 8, 11, 12) undergo larger deformations for a given horizontal force, producing wider hysteresis loops and thus superior energy absorption.

Fig. 17 corroborates the findings on the *x* direction and reveals an even more pronounced dichotomy in the *y* direction under quasi-static analysis, as seismic isolators beneath C2 (Joint 8, 9, 11, 12) columns consistently generate wider hysteresis loops and higher energy dissipation than the seismic isolators under C1 (Joints 1, 2, 3, 4, 5, 6, 7, 10, 13, 14, 15, 16) columns.

According to Figs. 16, 17, the analytical results demonstrate that under identical quasi-static

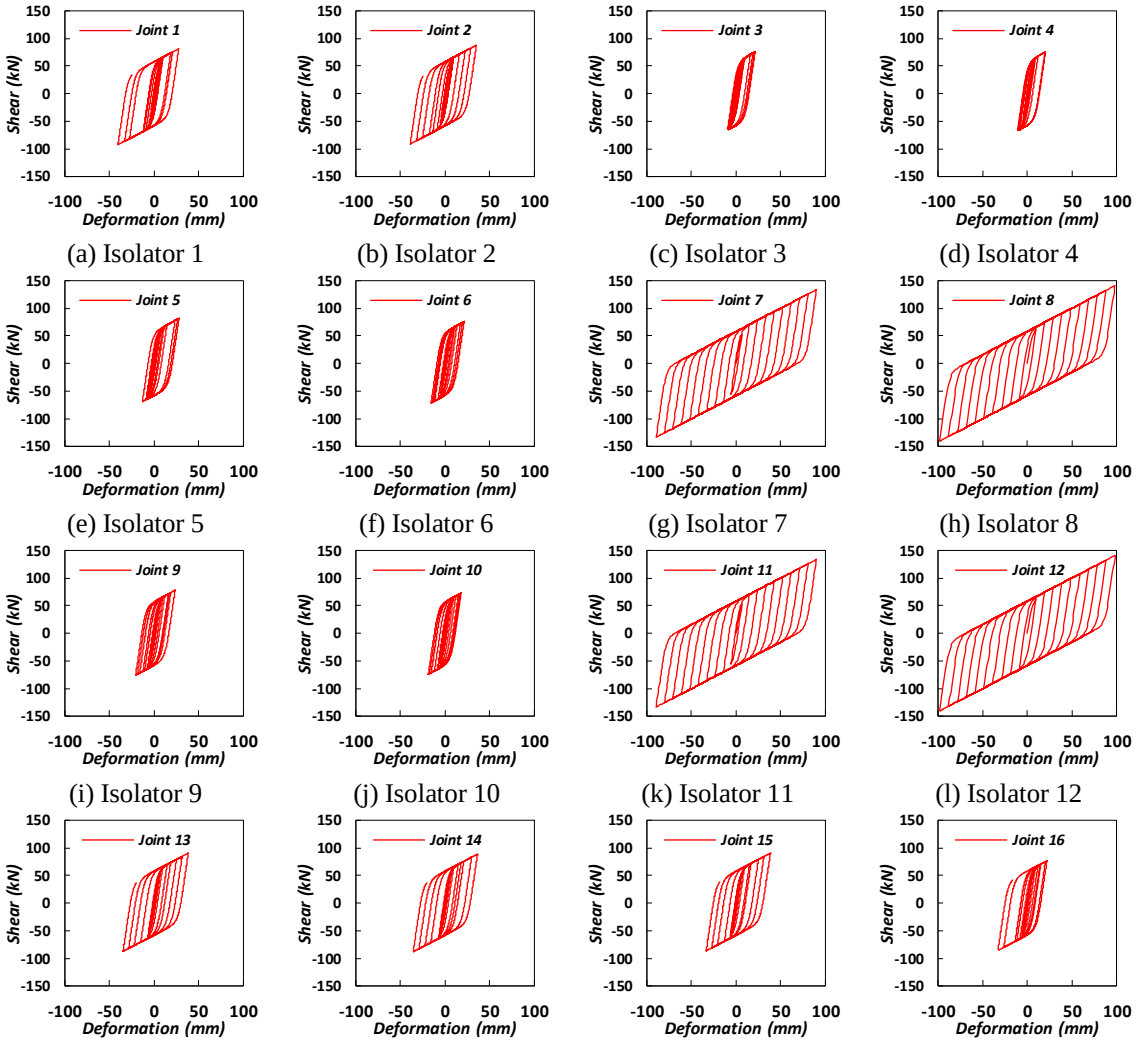

(a) Isolator 1 (b) Isolator 2 (c) Isolator 3 (d) Isolator 4

(e) Isolator 5 (f) Isolator 6 (g) Isolator 7 (h) Isolator 8

(i) Isolator 9 (j) Isolator 10 (k) Isolator 11 (l) Isolator 12

(m) Isolator 13 (n) Isolator 14 (o) Isolator 15 (p) Isolator 16

Figure 17. Behavior of seismic isolators in the *y* direction

loading protocols, all seismic isolators under Piloti-type RC columns exhibit clear hysteretic loops in both the *x* and *y* directions, signifying effective seismic energy dissipation. More specifically, even isolators paired with larger column sections incur higher vertical preloads that elevate their initial shear stiffness, but the seismic isolators expedite the transition into the sliding regime and widening loop areas due to the higher inertia, thereby increasing relative energy absorption. In contrast, even the seismic isolators beneath smaller column sections engage slide-plate mechanisms at lower shear thresholds, but the seismic isolators yield narrow loops due to the lower inertia. On the other hand, the analytical results on both analytical directions in Figs. 16, 17, by isolating the superstructure from ground motion, the seismic isolators not only dissipate energy efficiently but also capitalize on the separation effect to reduce inter-story drifts and foundation reactions, thereby enhancing overall seismic resilience.

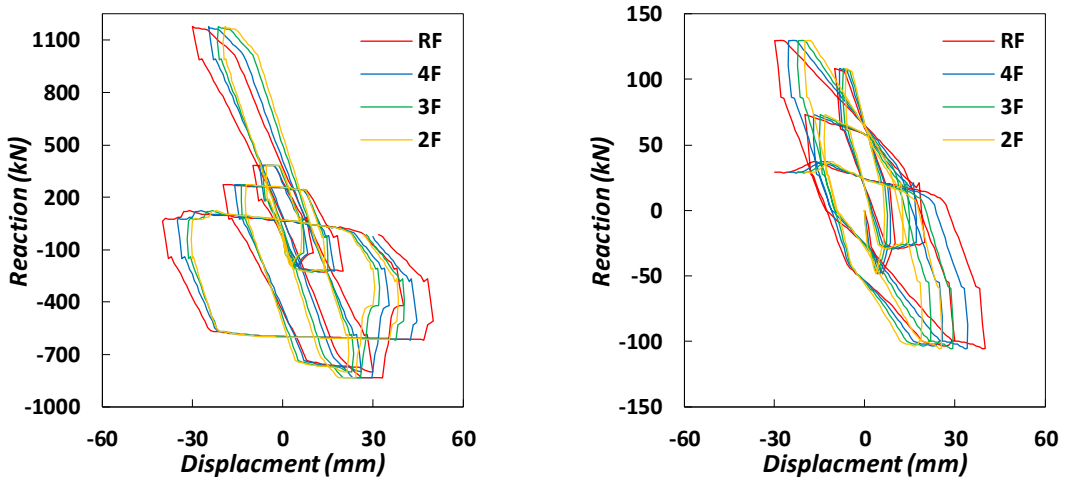

(a) Direction *x* (b) Direction *y*

Figure 18. Piloti-type RC structure without seismic isolator design

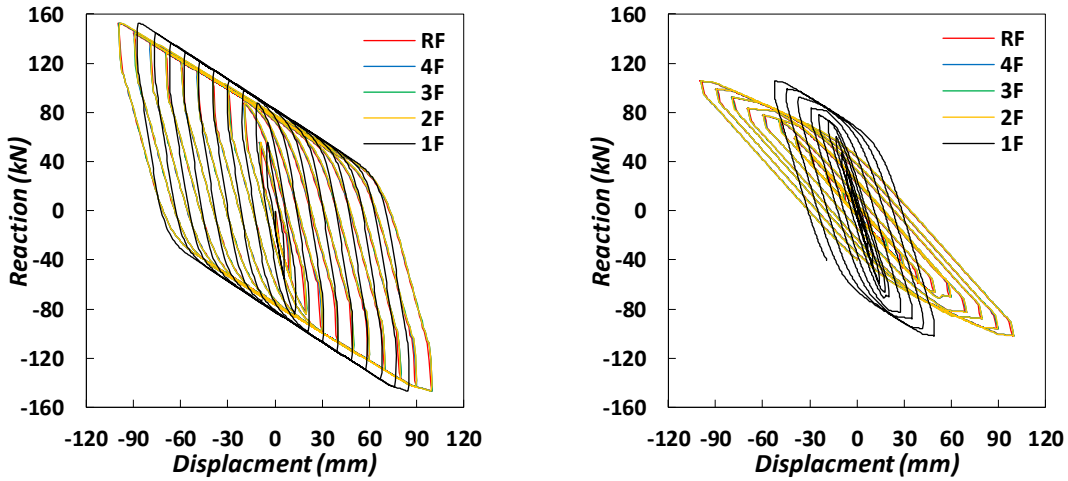

(a) Direction *x* (b) Direction *y*

Figure 19. Piloti-type RC structure with seismic isolator design

3.5 Reaction and displacement

In seismic performance assessment, the hysteretic curve of the base reaction force and story displacement provides a direct visualization of both the energy dissipation capacity and the stiffness degradation of a structure under cyclic loading [43]. In the quasi-static analysis of the Piloti-type RC building, these curves capture how the structure responds to incremental displacement demands, as a fuller loop indicates greater energy absorption through inelastic deformations, while a pinched or narrowed loop reveals stiffness and strength deterioration. In this study, Figs. 18, 19 contrast the hysteretic behavior of the Piloti-type RC structures without and with the seismic isolator design across different stories.

In the Piloti-type RC structure without the seismic isolator design of the quasi-static analysis in the *x* direction, the hysteretic response reveals both the ultimate load capacity and the progressive deterioration of lateral stiffness, as only 469 steps of the full 2,202 steps of displacement increments could be applied before global collapse. According to Fig. 18(a), the base reaction force peaks at 1,177.16 kN during the analysis of the 469 steps, highlighting the maximum inertial demand the structure can withstand before failure. Concurrently, the story displacements diminish gradually from the roof to the lower stories, with the roof level reaching 50 mm, the fourth floor 44.57 mm, the third floor 40.38 mm, and the second floor 38.42 mm.

On the other hand, in the *y* direction of the quasi-static analysis, only 351 steps of the 2,202 steps imposed displacement increments could be applied before total collapse, underscoring the limited deformation capacity without the seismic isolation more clearly. For the 351 steps of the quasi-static analysis in this study, the peak base reaction force reaches 129.68 kN as shown in Fig. 18(b), highlighting the maximum inertial demand transmitted through the ground-level columns prior to global instability. Concurrently, the maximum story displacements from roof to second floor as 40 mm at the roof level, 34.19 mm at the fourth floor, 29.34 mm at the third floor, and 25.49 mm at the second floor.

In the Piloti-type RC structure with the seismic isolator design under the quasi-static analysis on the *x* direction, the Piloti-type RC structure completes all 2,202 prescribed displacement steps without collapse, demonstrating the capacity of the seismic isolator to absorb inelastic demands and preserve superstructure integrity. According to Fig. 19(a), the peak base reaction force of 152.79 kN in the *x* direction, an order of magnitude lower than the peak of the Piloti-type RC structure without the seismic isolator design, indicates that the seismic isolator design effectively decouples seismic forces, reducing shear transmitted to the frame. Moreover, the near-uniform story displacements (100 mm at the roof, 99.95 mm at 4F, 99.94 mm at 3F, 99.83 mm at 2F, and 84.95 mm at 1F) reflect a rigid-body motion of the superstructure atop the isolation layer, which confines most deformation to the base.

As shown in Fig. 19(b), the hysteretic curves on the *y* direction of the Piloti-type RC structure with the seismic isolator design demonstrate full completion of all 2,202 quasi-static steps without collapse, underscoring the effectiveness of the seismic isolator design in both principal directions. According to Fig. 19(b), the peak base reaction force in the *y* direction is just 105.94 kN, markedly lower than the Piloti-type RC structure without the seismic isolator design, also confirming that the seismic isolator design decouples seismic energy from the superstructure and constrains shear demands at the foundation level in the *y* direction. Moreover, story displacements remain nearly uniform (100 mm at the roof, 99.91 mm at 4F, 99.80 mm at 3F, 99.74 mm at 2F, and only 49.25 mm at 1F) indicating a rigid-body translation of the frame atop the isolators and minimal inter-story drift in the superstructure on the *y* direction also.

Comparative analysis of hysteretic curves between the Piloti-type RC structures without and with the seismic isolator design, as depicted in Figs. 18, 19, reveals significant differences in seismic response characteristics. In both *x* and *y* directions, the Piloti-type RC structure without the seismic isolator design exhibits higher base reaction forces coupled with shorter story displacements, leading to premature collapse. Conversely, the Piloti-type RC structure with the seismic isolator design demonstrates lower base reaction forces and accommodates larger lateral displacements without collapse. This behavior underscores the efficacy of seismic isolation in enhancing structural resilience by decoupling the superstructure from ground motions, thereby reducing seismic demands and preventing early failure.

The energy dynamics captured in quasi-static analyses provide a fundamental insight to

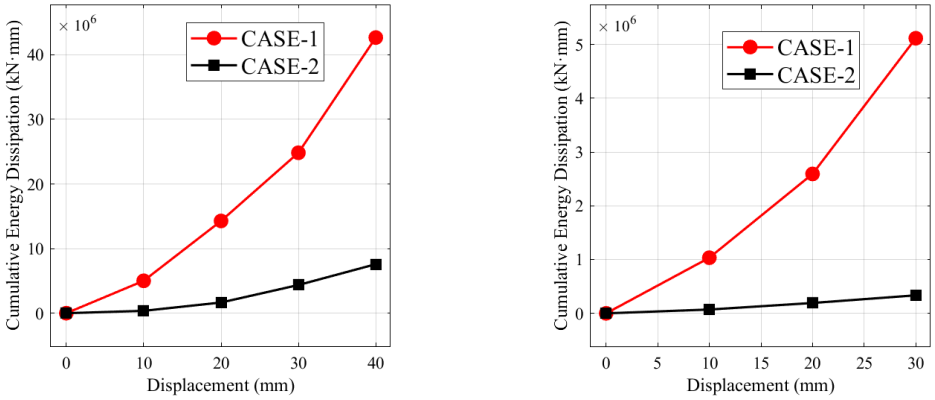

(a) Direction *x* (b) Direction *y*

Figure 20. Cumulative energy dissipation

evaluate RC frame resilience, emphasizing not just base shear or displacements, but the cumulative energy dissipation, which reflects how much seismic work the structure absorbs before damage occurs. Referring to the findings of Shi et al. [29] and Zhou et al. [44] underscore that a higher cumulative energy dissipation may indicate that the structure is absorbing excessive energy, often through inelastic deformations and plastic hinge rotation, which can precipitate damage.

The analysis of cumulative energy dissipation in this study is based by the earlier collapse behavior of the Piloti-type RC structure without the seismic isolator design because the structure without seismic isolation exhibited a premature formation of plastic hinges, leading to structural instability well before the completion of the full quasi-static analysis sequence as shown in the discussion of the plastic hinges. To ensure a consistent and meaningful comparison between the two structural configurations (without and with the seismic isolator designs), the cumulative energy dissipation assessment was limited to the displacement levels of 40 mm in the analytical direction *x* and 30 mm in direction *y*, as shown in Fig. 20.

Referring to the analytical results presented in Fig. 20, which compares the cumulative energy dissipation of the Piloti-type RC structure with and without the seismic isolator design, distinct trends emerge that highlight the effectiveness of seismic isolator design for the Piloti-type RC structure. Fig. 20(a) illustrates the energy dissipation in the *x* direction, while Fig. 20(b) presents the corresponding results in the *y* direction. The results indicate that the cumulative energy dissipation is consistently higher in the *x* direction than in the *y* direction for both structural configurations. This observation aligns with the inherent stiffness characteristics of the Piloti-type RC structure used in this study, which exhibits greater stiffness and consequently higher energy absorption capacity along the *x* axis. When comparing the structures with and without seismic isolator design, it is evident that the structure without the isolator design dissipates more energy directly through the RC frame, which results in a larger internal energy demand and increased plastic deformation. Conversely, the Piloti-type RC structure with the seismic isolator design demonstrates a markedly different behavior as the energy is primarily absorbed by the seismic isolators through deformation and shear, transforming seismic input into hysteretic energy, and reducing demand on the superstructure.

The findings in this study emphasize that the redirection of energy dissipation from the RC frame to the isolators is critical in preventing widespread plastic hinge formation and delaying

structural collapse. The capacity of the seismic isolators to absorb energy effectively reduces the cumulative energy that the Piloti-type RC structure must withstand, safeguarding the structural integrity of the upper stories. Therefore, the reduced cumulative energy dissipation observed in the seismic isolated Piloti-type RC structure is not indicative of poorer performance, but rather of an optimized energy distribution mechanism that improves the structural seismic resilience, and these findings underscore the importance of seismic isolators as a key strategy in mitigating damage from seismic activities.

4. Summarization

This study comprehensively evaluated the seismic performance of a representative piloti-type RC building (Ministry of Land, Infrastructure and Transport, R.O.K.) to quantify the efficacy of seismic isolation. Utilizing displacement-controlled quasi-static analyses, the structural responses of non-isolated and base-isolated configurations were systematically compared. The evaluation focused on critical performance indicators, including plastic hinge evolution, lateral displacement profiles, inter-story drift ratios, base shear reactions, and energy dissipation mechanisms, yielding the following principal findings:

First, the implementation of seismic isolation fundamentally mitigates severe structural damage by altering the plastic hinge progression. The quasi-static analysis in this study confirmed that the non-isolated piloti RC structure exhibits high susceptibility to localized failure, with plastic hinges rapidly degrading into the Collapse Prevention (CP) state. In stark contrast, the base-isolated counterpart successfully arrested hinge development at significantly lower performance thresholds, entirely preventing structural elements from reaching the CP state and thereby preserving the life-safety performance of the primary gravity-load-carrying frame.

Second, the isolation system effectively decouples the superstructure from the foundation on the ground, leading to highly controlled and predictable kinematic responses. The base-isolated configuration demonstrated substantially reduced inter-story drift ratios across all structural levels. This attenuation of drift is critical for piloti-type architectures, as it not only prevents the formation of catastrophic soft-story mechanisms at the ground level but also minimizes potential damage to non-structural components, thereby maintaining the overall functional integrity of the building during seismic events.

Third, the reaction force-displacement behavior explicitly validates the load-reduction capabilities of the isolation design. Structures equipped with seismic isolators accommodated larger structural lateral displacements while simultaneously registering significantly lower base reaction forces. On the other hand, the non-isolated structures exhibited a much stiffer structural response characterized by higher base shear demands and restricted displacement capacities. Upon the discussion above, such pronounced reduction in transmitted forces confirms that the isolators effectively filter seismic influences before they propagate into the vulnerable superstructure.

Fourth, the analysis in this study revealed that the efficiency of energy dissipation is highly dependent on both the directional stiffness of the structure and the geometric sizing of specific structural components. The findings in this study emphasize that energy absorption was found to be notably more pronounced along the stiffer structural axis (the *x* direction), dictating the primary pathways for energy dissipation. Furthermore, the integration of larger column sections (C2) working in tandem with the isolators enhanced the overall hysteretic energy absorption capacity compared to smaller column designs (C1). Due to this, this study demonstrates that optimizing

isolator performance requires a synergistic approach that actively accounts for the asymmetric stiffness and component dimensions of the superstructure.

In conclusion, this study underscores the critical necessity and strategic application of seismic isolators for piloti-type RC structures, which are inherently vulnerable to soft-story collapse. By effectively decoupling the structure from seismic energy, controlling drift, and synergizing with appropriately sized column elements, seismic isolation transitions these high-risk buildings from conventional life-safety compliance toward advanced seismic resilience. From the perspective of practice as emphasized in Du et al. [45], tailoring isolation strategies to specific directional stiffness and architectural configurations provides a robust framework for retrofitting and designing piloti-type RC structures, safeguarding urban dwellings and promoting the sustainable resilience of the built environment.

5. Conclusions

The comprehensive quasi-static evaluation conducted in this study demonstrates that seismic isolation is an indispensable strategy for mitigating the catastrophic collapse risk inherent in piloti-type RC structures. The analysis in this study reveals that while non-isolated configurations are critically vulnerable to localized soft-story mechanisms, the integration of lead-rubber bearings effectively reconfigures the structural demand. By decoupling the superstructure from seismic forces, the isolation system not only preserves the elastic integrity of the gravity-load-carrying elements but also standardizes the inter-story drift profile. Furthermore, the findings highlight a crucial synergy between isolator efficiency and the directional stiffness and column sizing of the superstructure, suggesting that seismic resilience is optimized when isolation strategies are tailored to the specific geometric and mechanical asymmetries of the piloti-type RC structures.

This study provides significant contributions to the fields of structural seismic isolation and performance-based design. The analysis in this study establishes a reproducible framework for utilizing displacement-controlled quasi-static analysis to describe the non-linear hinge evolution and energy absorption pathways in complex, irregular RC frames. By explicitly quantifying the interaction between directional stiffness and isolator hysteretic behavior, this work offers practical engineering guidance for the retrofitting and design of high-density urban dwellings. The findings in this study facilitate a transition from conventional life-safety objectives toward advanced seismic resilience, ensuring that piloti-type structures can maintain functionality and structural stability under severe seismic demands.

Despite the insights gained, even the quasi-static approach employed in this study is effective for mapping capacity and collapse progression, but cannot fully account for the rate-dependent effects and complex damping characteristics inherent in real-world seismic events. To address these limitations, future research should incorporate non-linear time-history analyses (NTHA) using site-specific measured ground motions. Transitioning from static capacity curves to dynamic time-domain simulations is expected to allow for a more nuanced understanding of the structure's kinetic energy response and the potential for higher-mode effects. According to the foundational interaction patterns identified in this study, such advancements are expected to refine the precision of seismic isolation applications and promote the long-term sustainable resilience of the piloti-type RC structures.

Acknowledgements

This research was supported by the 25th Batch High-Level Talent Research Project of Ankang University, “Seismic Response and Collapse Mechanisms of RC Structures via Deep Learning–Finite Element Coupling” (2026AYQDZR27).

References

1. Shin, J., Lee, H., Min, J.K., Choi, I.R., Choi, S.M. (2022). Predicting temperature loads in open car parks of piloti structures exposed to real fire accidents. International Journal of Steel Structures, 22(6), 1889-1907. https://doi.org/10.1007/s13296-022-00675-2.
2. Hahn, S., Choi, I., Chang, H., Kim, J. (2025). Development of seismic fragility framework for piloti-type buildings based on structural parameters. Journal of the Earthquake Engineering Society of Korea, 29(1_spc), 91-97. https://doi.org/10.5000/EESK.2025.29.1.091.
3. Lee, H.S., Ko, D.W. (2002). Shaking table tests of a high-rise RC bearing-wall structure with bottom piloti stories. Journal of Asian Architecture and Building Engineering, 1(1), 47-54. https://doi.org/10.3130/jaabe.1.47.
4. Wang, F., Zhang, J., Liu, W., Zhao, D., Cao, W. (2024). Seismic behavior of rehabilitated recycled aggregate piloti-type structure reinforced with ultra-high strength bars. Journal of Building Engineering, 84, 108673. https://doi.org/10.1016/j.jobe.2024.108673.
5. Zhang, J., Wang, F., Zhao, D., Zhang, M., Cao, W. (2023). Seismic performance of resilient recycled aggregate piloti-type structure employing ultra-high strength bars. Engineering Structures, 282, 115795. https://doi.org/10.1016/j.engstruct.2023.115795.
6. Nascimbene, R. (2024). Investigation of seismic damage to existing buildings by using remotely observed images. Engineering Failure Analysis, 161, 108282. https://doi.org/10.1016/j.engfailanal.2024.108282.
7. Kim, T., Park, J.H., Yu, E. (2023). Seismic fragility of low-rise piloti buildings based on 2017 Pohang earthquake damage. Journal of Building Engineering, 76, 107032. https://doi.org/10.1016/j.jobe.2023.107032.
8. Yang, J., Sun, S., Tian, T., Li, W., Du, H., Alici, G., Nakano, M. (2016). Development of a novel multi-layer MRE isolator for suppression of building vibrations under seismic events. Mechanical Systems and Signal Processing, 70, 811-820. http://doi.org/10.1016/j.ymssp.2015.08.022.
9. Kang, B.S., Li, L., Ku, T.W. (2009). Dynamic response characteristics of seismic isolation systems for building structures. Journal of Mechanical Science and Technology, 23, 2179-2192. http://doi.org/10.1007/s12206-009-0437-x.
10. Warn, G.P., Ryan, K.L. (2012). A review of seismic isolation for buildings: historical development and research needs. Buildings, 2(3), 300-325. http://doi.org/10.3390/buildings2030300.
11. Blanford, E., Keldrauk, E., Laufer, M., Mieler, M., Wei, J., Stojadinovic, B., Peterson, P.F. (2010). Advanced seismic base isolation methods for modular reactors. No. DOE/ID/14923, University of California Berkeley.
12. Shi, M., Choi, M., Choi, Y. (2025). A comparative research of the Piloti-type RC structure and non-Piloti-type RC structure under the nonlinear pushover analysis. Building Engineering, 3(1), 1834-1834. https://doi.org/10.59400/be1834.
13. Harris, J., Speicher, M. (2018). Assessment of performance-based seismic design methods in ASCE 41 for new steel buildings: special moment frames. Earthquake Spectra, 34(3), 977-999. https://doi.org/10.1193/050117EQS079EP.
14. Han, S.W., Lee, C.S., Paz Zambrana, M.A., Lee, K. (2019). Calibration factor for ASCE 41-17 modeling parameters for stocky rectangular RC columns. Applied Sciences, 9(23), 5193. https://doi.org/10.3390/app9235193.

15. Choi, K.K., Kim, J.C. (2015). Seismic capacity of rc structures with non-seismic details and standard details for structural retrofit. Magazine of the Korea Concrete Institute, 27(6), 31-35. https://doi.org/10.22636/MKCI.2015.27.6.31.
16. Inel, M., Ozmen, H.B. (2006). Effects of plastic hinge properties in nonlinear analysis of reinforced concrete buildings. Engineering Structures, 28(11), 1494-1502. https://doi.org/10.1016/j.engstruct.2006.01.017.
17. Pham, T.M., Hao, H. (2017). Plastic hinges and inertia forces in RC beams under impact loads. International Journal of Impact Engineering, 103, 1-11. https://doi.org/10.1016/j.ijimpeng.2016.12.016.
18. Di Ludovico, M., Polese, M., d'Aragona, M.G., Prota, A., Manfredi, G. (2013). A proposal for plastic hinges modification factors for damaged RC columns. Engineering Structures, 51, 99-112. https://doi.org/10.1016/j.engstruct.2013.01.009.
19. Zhao, X.M., Wu, Y.F., Leung, A.Y.T. (2012). Analyses of plastic hinge regions in reinforced concrete beams under monotonic loading. Engineering Structures, 34, 466-482. https://doi.org/10.1016/j.engstruct.2011.10.016.
20. Shahrouzi, M., Ebadijalal, M. (2023). A deductive design method to simplify ASCE 41-17 nonlinear static procedure preserving the adjusted collapse margin ratio of steel moment frames. Asian Journal of Civil Engineering, 24(3), 657-671. https://doi.org/10.1007/s42107-022-00522-z.
21. Hakhamaneshi, M., Kutter, B.L., Gavras, A.G., Gajan, S., Tsatsis, A., Liu, W., ... Gazetas, G. (2020). Database of rocking shallow foundation performance: Slow-cyclic and monotonic loading. Earthquake Spectra, 36(3), 1585-1606. https://doi.org/10.1177/8755293020906564.
22. El Hoseny, M., Forcellini, D., Ma, J. (2024). The role of the foundation gap on the pounding between low-rise buildings. Structures, 63, 106412. https://doi.org/10.1016/j.istruc.2024.106412.
23. Khamesi, S.O., Hosseini, S.M.M.M. (2023). A numerical study of influential parameters on rocking response of shallow foundations of single degree of freedom (SDOF) structures. Journal of Engineering Research, 11(2), 100055. https://doi.org/10.1016/j.jer.2023.100055.
24. Chen, P., Wang, B., Zhang, Z., Li, T., Dai, K. (2023). A generalized model of lead rubber bearing considering large strain stiffening and degradation. Engineering Structures, 275, 115264. https://doi.org/10.1016/j.engstruct.2022.115264.
25. Ju, S.H., Yuantien, C.C., Hsieh, W.K. (2020). Study of lead rubber bearings for vibration reduction in high-tech factories. Applied Sciences, 10(4), 1502. https://doi.org/10.3390/app10041502.
26. Pourmasoud, M., Hajirasouliha, I., Park, A., Lim, J.B.P. (2022). A new approach to estimate the lead core characteristic strength of lead rubber bearings. Engineering Structures, 270, 114817. https://doi.org/10.1016/j.engstruct.2022.114817.
27. Yasar, C., Karuk, V., Cavdar, E., Ozdemir, G. (2024). Modifications in both lead and rubber properties of LRBs at low temperatures considering the size effect. Engineering Structures, 307, 117902. https://doi.org/10.1016/j.engstruct.2024.117902.
28. Koo, G.H., Jung, J.Y., Lee, J.H., Shin, T.M., Park, J.Y. (2020). Development of small-sized lead inserted laminated rubber bearing for nuclear component seismic isolation. Energies, 13(12), 3193. https://doi.org/10.3390/en13123193.
29. Shi, M., Choi, Y., Kang, S. (2023). A study of the infill wall of the RC frame using a quasi-static pushover analysis. Computers and Concrete, 32(5), 455-464. https://doi.org/10.12989/cac.2023.32.5.455.
30. Abass, H.A., Jarallah, H.K. (2021). Comparative study of the seismic assessment according to ATC-40, FEMA-356 and FEMA-440 for existing hospital building located at Baghdad City.
31. Ní Choine, M., O'Connor, A.J., Padgett, J.E. (2015). Comparison between the seismic performance of integral and jointed concrete bridges. Journal of Earthquake Engineering, 19(1), 172-191. https://doi.org/10.1080/13632469.2014.946163.
32. Ferraioli, M., Mandara, A. (2017). Base isolation for seismic retrofitting of a multiple building structure: design, construction, and assessment. Mathematical Problems in Engineering, 2017(1), 4645834. https://doi.org/10.1155/2017/4645834.
33. Lou, X., Huang, Y., Lv, Y., Huang, Q. (2022). Seismic performance of the series seismic isolation systems designed by the procedures of GB50011-2010 and ASCE/SEI 7-16. Case Studies in

Construction Materials, 17, e01184. https://doi.org/10.1016/j.cscm.2022.e01184.
34. Fakih, M., Hallal, J., Darwich, H., Damerji, H. (2021). Effect of lead-rubber bearing isolators in reducing seismic damage for a high-rise building in comparison with normal shear wall system. Structural Durability & Health Monitoring, 15(3), 247. https://doi.org/10.32604/sdhm.2021.015174.
35. Sahoo, D.N., Parhi, P.K. (2018). Base isolation of residential building using lead rubber bearing technique. International Journal of Engineering Research & Technology (IJERT), 7(05), 122-131.
36. Komur, M.A. (2016). Soft-story effects on the behavior of fixed-base and LRB base-isolated reinforced concrete buildings. Arabian Journal for Science and Engineering, 41, 381-391. https://doi.org/10.1007/s13369-015-1664-3.
37. Gong, M., Zuo, Z., Wang, X., Lu, X., Xie, L. (2019). Comparing seismic performances of pilotis and bare RC frame structures by shaking table tests. Engineering Structures, 199, 109442. https://doi.org/10.1016/j.engstruct.2019.109442.
38. Shin, J., Choi, I., Kim, J. (2021). Rapid decision-making tool of piloti-type RC building structure for seismic performance evaluation and retrofit strategy using multi-dimensional structural parameter surfaces. Soil Dynamics and Earthquake Engineering, 151, 106978. https://doi.org/10.1016/j.soildyn.2021.106978.
39. Ma, X.T., Bao, C., Doh, S.I., Lu, H., Zhang, L.X., Ma, Z.W., He, Y.T. (2021). Dynamic response analysis of story-adding structure with isolation technique subjected to near-fault pulse-like ground motions. Physics and Chemistry of the Earth, Parts A/B/C, 121, 102957. https://doi.org/10.1016/j.pce.2020.102957.
40. Amini, A.R.B., Narjabadifam, P., Asl, G.R.O., Emamverdi, S., Derogar, S., Ozarisoy, B. (2025). Assessing the threshold of need for supplemental damping in seismic base isolation of multistory buildings. Shock and Vibration, 2025(1), 4576020. https://doi.org/10.1155/vib/4576020.
41. Forcellini, D., Kalfas, K.N. (2025). A framework to quantify the impact of deterioration on the seismic resilience of structures. Structure and Infrastructure Engineering, 1-9. https://doi.org/10.1080/15732479.2025.2591824.
42. Liao, J., Forcellini, D., Fang, J., Sun, L. (2026). An entropy-based multi-criteria approach for intensity measure selection in seismic resilience of structures. Resilient Cities and Structures, 5(1), 1-13. https://doi.org/10.1016/j.rcns.2025.12.005.
43. Pavese, A., Lanese, I., Nascimbene, R. (2017). Seismic vulnerability assessment of an infilled reinforced concrete frame structure designed for gravity loads. Journal of Earthquake Engineering, 21(2), 267-289. https://doi.org/10.1080/13632469.2016.1172372.
44. Zhou, X., Kou, X., Peng, Q., Cui, J. (2018). Influence of infill wall configuration on failure modes of RC frames. Shock and Vibration, 2018(1), 6582817. https://doi.org/10.1155/2018/6582817.
45. Du, A., Wang, X., Xie, Y., Dong, Y. (2023). Regional seismic risk and resilience assessment: Methodological development, applicability, and future research needs–An earthquake engineering perspective. Reliability Engineering & System Safety, 233, 109104. https://doi.org/10.1016/j.ress.2023.109104.